Equivalent Circuit Determination of Inductive Voltage Transformers Based on Impedance Analysis

Abdelkrim KISSERLI[AB], Mathieu ROSSI[B], Josué DELVILLE[A], Sylvain LEFEBVRE[A], Stéphane DUCHESNE[B]
[A] SADTEM, 671 Rue Maurice Caullery, 59500 Douai.
[B] Univ. Artois, UR 4025, Laboratoire Systèmes Electrotechniques et Environnement (LSEE), Béthune, F-62400, France

Abstract – This study investigates the frequency response of Inductive Voltage Transformers (IVTs) by analyzing their impedance across a range of test conditions and frequencies. The impedance measurement approach employed in this work is adapted from a well-established method initially developed for high-frequency transformers (typically operating above 100 kHz), offering an innovative application to a new class of low-frequency transformers (operating below 100 kHz). This extension not only demonstrates the versatility of the method but also provides a valuable basis for comparison with impedance analysis of similar transformers conducted using alternative techniques. While the focus of this comparison is not primarily on numerical results, the conclusions derived from both studies reveal new perspectives and raise critical questions for further exploration in the field.

Key Words—Instrument Transformers, Voltage Transformers, Harmonics, Frequency Analysis, Impedance Measurment, Equivalent Circuit..

1. INTRODUCTION

Measuring harmonics has become a critical concern for energy providers due to the declining quality of power in electrical grids. This decline is attributed to significant changes in grid infrastructure, including the extensive integration of renewable energy sources and the emergence of unconventional loads, such as electric vehicle chargers. IVTs are typically used to monitor voltage and prevent failures in power grids at standard frequencies of 50/60 Hz with high accuracy. However, their performance in measuring harmonics presents notable challenges.

Studies [1] have shown that IVTs may experience a considerable loss of accuracy when measuring harmonics. This loss is often accompanied by the presence of resonance phenomena, primarily caused by the emergence of capacitive effects at high frequencies interacting with the transformer's inherent inductive behavior. To characterize these phenomena effectively, it is crucial to establish an equivalent circuit model for the transformer at high frequencies. Such a model helps in understanding the phenomena, identifying the limitations of the standard 50/60 Hz model, and forming the foundation for more advanced modeling approaches.

Several characterization methods have been developed to determine high-frequency models, emphasizing the use of inductive transformers in power conversion applications rather than in transmission. Among these methods, the technique presented in [2, 3] provides a detailed procedure for determining an n-winding high-frequency model with constant variables. This method begins with impedance measurements conducted using an impedance analyzer.

Furthermore, a recent study [4] has investigated a typical high-frequency model based on voltage-current measurements across a range of frequencies, associated to 2D finite element method (FEM) simulations. This approach provides deeper insights into transformer behavior under conditions shaped by modern grid requirements.

There is growing interest in improving the bandwidth of IVTs to enable accurate Power Quality (PQ) measurements. Understanding the phenomena and identifying the limitations of the equipment are critical steps that include the improvement of the IVT equivalent circuit for a more accurate representation at high frequencies.

A well-established method for determining the equivalent circuit of transformers was employed to analyze a wide range of IVT prototypes with varying characteristics. Originally developed for high-frequency transformers—such as those used in power electronic converters with resonance frequencies above 100 kHz—this method is here applied to low-frequency transformers like IVTs, which typically exhibit resonance phenomena below 1 kHz. Our study demonstrates the method's reliability in this new context and provides meaningful insights by comparing the results, highlighting consistent modeling behavior across frequency domains.

The impedance analysis method has also been applied in other contexts to study the behavior of IVTs, albeit with different procedures. The results reported in [4] are similar to those obtained with our method, but the conclusions differ. This difference is primarily attributed to the extensive range of prototypes tested in our study, which allowed for a clearer understanding of the phenomena and offered more accurate explanations for certain observations.

The paper is organized as follows: section 2. Measurement procedure, section 3. Determination of equivalent circuit, section 4. Prototyping strategy, section 5. Tests and results, section 6. Modeling discussion and comparison and finally, section 7. Conclusion.

2. MEASURMENT PROCEDURE

2.1. Test Equipment

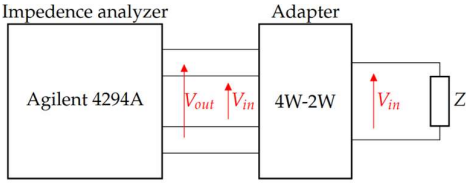

Fig.1. Impedance analysis circuit diagram.

Figure 1 shows the circuit diagram for impedance analysis used to carry out the frequency sweep. The impedance analyzer employed is an Agilent 4294A, capable of measuring impedances ranging from $\mu\Omega$ to $M\Omega$ over a frequency range of 40 Hz to 110 MHz. A 4-wire to 2-wire adapter is used to facilitate the measurement procedure.

2.2. *Equivalent circuits overview*

The test procedure is based on a localized constant approach. This approach assumes an equivalent circuit, followed by determining the parameters of each element. According to [5], separating magnetic energy from electrostatic energy results in an inductive and capacitive equivalent circuit connected in parallel, as shown in figures 2.

The inductive system consists of the primary and secondary resistances r_p and r_s, the impedance z_p associated with the magnetizing branch and z_s representing the leakage impedance. Finally, η is the transformation ratio. The capacitive system includes three components: primary, secondary and inter winding capacitances $C_1, C_2$and C_3 respectively.

The parameter identification process is carried out in two main steps: first, the inductive elements are determined, followed by the capacitive ones.

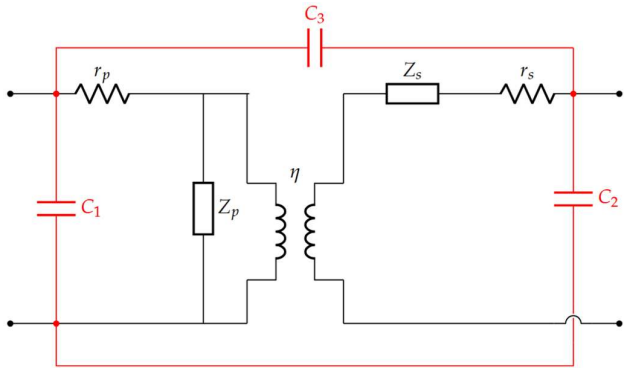

Fig.2. Inductive equivalent circuit (in black) and capacitive equivalent circuit (in red)

3. DETERMINATION OF EQUIVALENT CIRCUIT

3.1. *Inductive equivalent circuit*

Four main tests will be carried out, as illustrated in the figure 4.

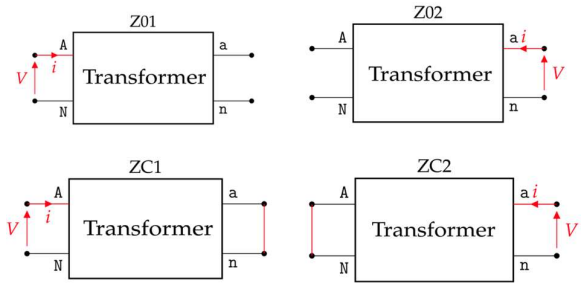

Fig.3. Test setups for inductive circuit parameters extraction

AN and **an** represent the primary and secondary coil terminals, respectively. Each coil will be tested twice: once with the other coil in an open-circuit condition and once in a short-circuit condition.

The formulation of the parameters is given as follows:

$$\eta = \frac{\sqrt{Z02(Z01 - ZC1)}}{Z01 - r_p} \tag{1}$$

$$Z_p = Z01 - r_p \tag{2}$$

$$Z_s = \frac{Z02(Z01 - r_p)}{Z01 - r_p} - r_s \tag{3}$$

The resistances r_p and r_s will be determinate via direct ohmic measurement of the primary and secondary windings.

3.2. *Capacitive equivalent circuit*

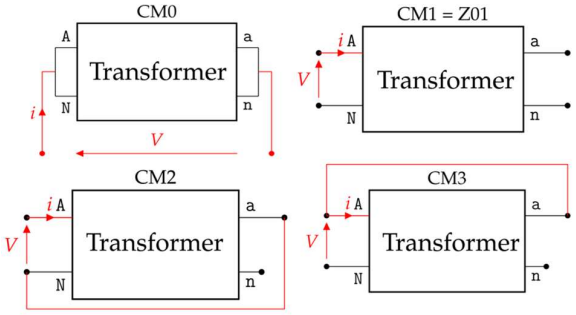

Fig.4. Test setups for capacitive circuit parameters extraction

The capacitive equivalent circuit is determined based on the four test configurations illustrated in the figure 5. The principle of the test method involves selectively short-circuiting specific capacitances to preserve the maximum number of parallel-connected elements. This approach facilitates the formulation and resolution of the system of equations presented below.

$$\begin{aligned} CM0 &= C_2 + C_3 \\ CM1 &= C_1 + C_3 \\ CM2 &= C_1 \ + C_2 \\ CM3 &= C_1 + \frac{C_3.C_2}{C_3 + C_2} \end{aligned} \tag{4}$$

4. PROTOTYPING STRATEGY

To establish a solid foundation for comparison, five prototypes were manufactured based on specific production characteristics and transformer standards. This approach ensured a significant variation in their inductive and capacitive properties. As a reference, a prototype IVT with a 10 kV // 100 V voltage ratio, 0.2 accuracy class, 10 VA rated power, and a power factor of cos(φ) = 0.8 was manufactured. This reference IVT (figure 6) reflects a typical design corresponding to standard customer requirement. The primary winding consists of 26951 turns arranged over 55 layers, while the secondary winding consists 270 turns arranged over 4 layers. The core cross-sectional area is 16.3 cm².

Fig.5. Picture of prototype transformer

The next step was to develop derivative prototypes based on the reference design, without affecting the main function which is the 10 kV // 100 V transformation ratio and the 0.2 accuracy class. By acting on specific manufacturing processes. The specifications of the prototypes are described in the table below.

Table 1. List of derivative prototypes and their specifications.

Prototype	**Specification**
A	Reference
B	Larger winding frame
C	Thicker primary/secondary insulation layer
D	Use of nanocrystalline core
E	Reduced number of coil turns by 50% , compensated by a larger core cross-sectional area

Prototype B is intended to study the effect of increasing the distance between the coils and the magnetic core. Prototype C is designed to reveal the influence of insulation thickness on the dielectric spacing between the primary and secondary windings. Prototype D is a key variant, as it incorporates a high-permeability material which is the nanocrystalline core known for its low losses and high-frequency performance. Prototype E directly addresses the impact of reducing the number of turns, compensated by a larger core cross-sectional area.

5. TESTS AND RESULTS

5.1. Measurment results

After completing all the measurement tests, which consist of seven different configurations, the results are presented in figure 7.

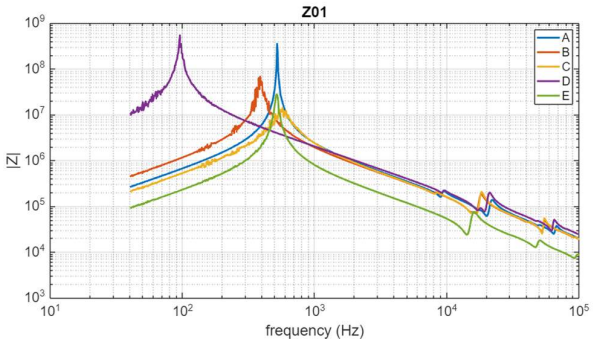

Fig.6.1. Test Z01

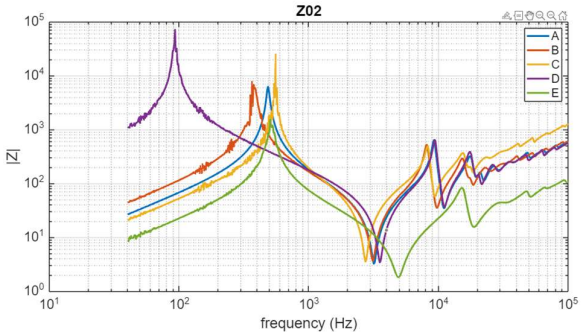

Fig.6.2. Test Z02

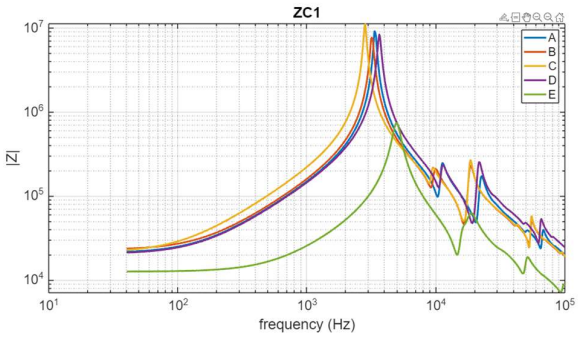

Fig.6.3. Test ZC1

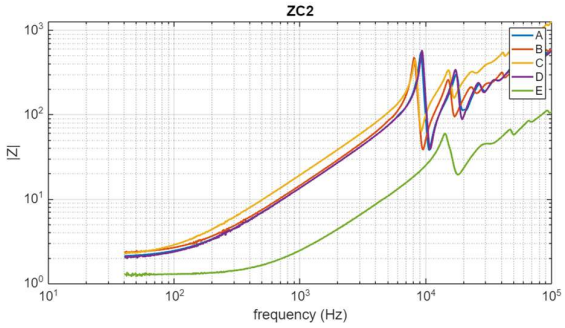

Fig.6.4. Test ZC2

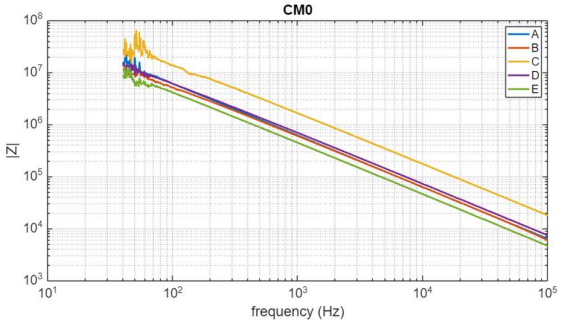

Fig.6.5. Test CM0

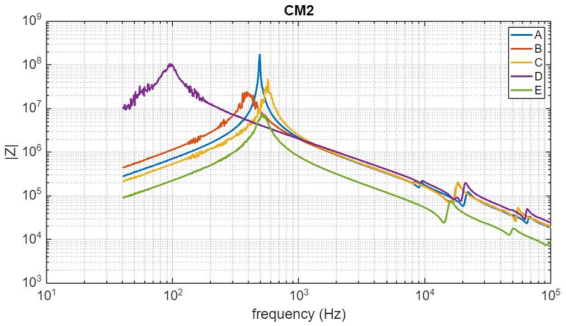

Fig.6.6. Test CM2

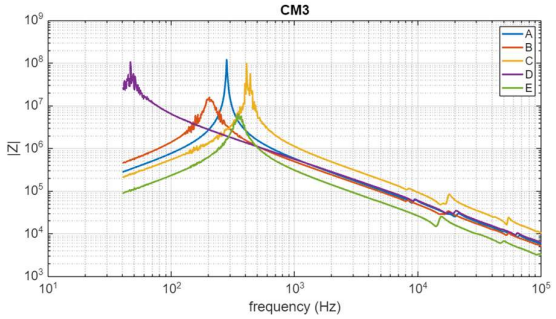

Fig.6.7. Test CM3

5.2. *Measurments interpretation*

Before analyzing the modeling, it is useful to highlight some key observations directly from the measurements. Prototype D, which uses a nanocrystalline core with high permeability, exhibits an inductance approximately 40 times greater as shown in figure 6.1, compared to prototypes using silicon steel cores. However, the capacitance value remains unchanged. In Prototype C, where the thickness of the insulation layer between the primary and secondary windings was increased, a lower capacitance is observed in measurement CM0 (figure 6.5), reflecting reduced coupling between the windings. Prototype E, in which the number of turns was halved, shows a general fourfold decrease (divided by four) in impedance across nearly all measurements. Other prototype variations introduce some changes in the results, but their impact remains minor compared to these dominant effects.

5.3. *Case Study: Applying the Calculation Method*

To provide a better understanding of how the method operates and how the data is processed to determine the equivalent circuit, all calculations will be performed using prototype A as a case study. The method will be validated at the end.

5.3.1. *Inductive quadripole. Z_p, Z_s and η*

First, Z_p is calculated using equation (2). Then, the RLC parameters are determined. As observed in figure 7, the behavior of the magnetizing branch can be accurately modeled using an RLC parallel circuit, with the following component values from figure 8. Apart from that, since we are dealing with the inductive circuit, capacitance is not explicitly included in Z_p, and it won't appear in the final inductive model even if it is present. It will naturally emerge from the capacitive model.

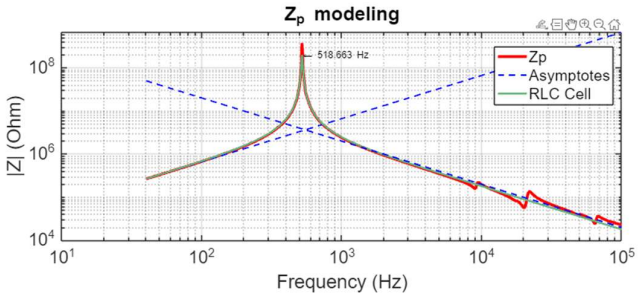

Fig.7. Z_p calculation and equivalent RLC cell representation

R_m $[M\Omega]$	400
L_m $[H]$	1048
C $[pF]$	80.45

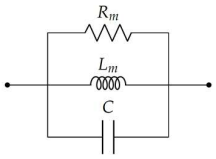

Fig.8. Equivalent RLC representation of Z_p with parameter values

Next, Z_s is determined using the same procedure, based on Equation (3). Since the response does not exhibit any resonance phenomena, the system can be considered purely inductive. Two asymptotic behaviors can be observed in figure 9: one at low frequencies (below 10 kHz) and another at high frequencies (above 100 kHz), likely corresponding to the effect of two distinct inductive cells, as represented in figure 10. These phenomena are commonly attributed to skin effect and proximity effect, which become more significant at higher frequencies and influence the apparent inductance.

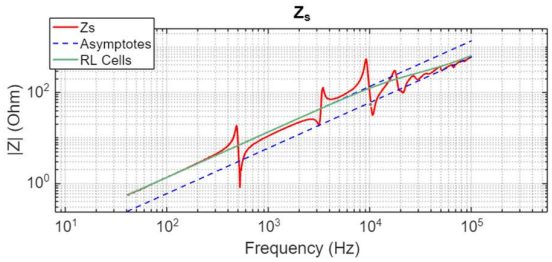

Fig.9. Z_s calculation and equivalent RL cell representation

R_m $[\Omega]$	150
L_{BF} $[mH]$	2.15
L_{HF} $[mH]$	0.95

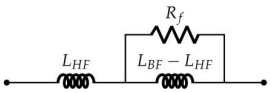

Fig.10. Equivalent RL representation of Z_s with parameter values

Finally, η will be represented by its inverse, $k = \frac{1}{\eta}$, to align with the transformer's turns ratio, which is equal to 100.

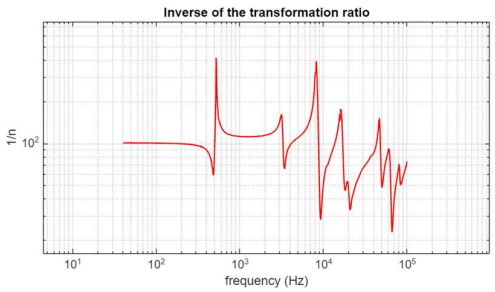

Fig.11. Ratio η calculation

5.3.2. *Capacitive quadripole. C_1, C_2 and C_3*

The determination of C_1, C_2 and C_3 differs from the previous method. It is based on solving the system of equations (4), using the values $CM0, CM1, CM2$ and $CM3$. These values are obtained by evaluating the impedance in the descending part of the frequency response curve, which reflects the capacitive behavior. In this case, the system includes four equations for three unknowns. The fourth equation, corresponding to CM3, is specifically used as a validation point to assess the consistency of the model.

Table 2.Capacitances values.

C_1 $[pF]$	59.17
C_2 $[pF]$	224.43
C_3 $[pF]$	28.42

5.3.3. *Method validation*

To validate the method, a circuit simulation was conducted, as shown in figure 12, to reproduce the impedance behavior over a range of frequencies up to 100 kHz. The electrical circuit is solved directly by expressing it in matrix form, where the circuit's admittances are clearly defined.

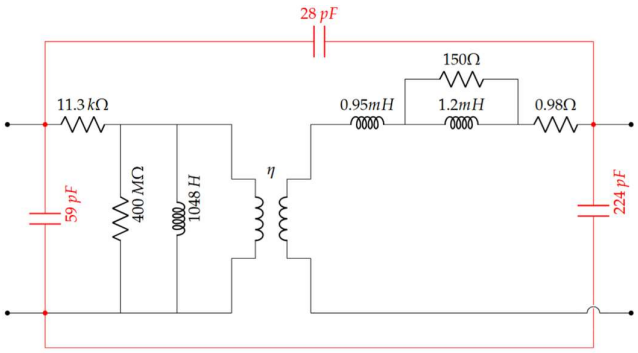

Fig.12. Simplified validation circuit implemented

As shown in figure 13, the model performs well under no-load as well as loaded conditions, whether observed from the primary or secondary side of the transformer. The behavior is accurately modeled up to 10 kHz. A more complete model including more capacitors would likely capture additional resonances beyond this frequency range.

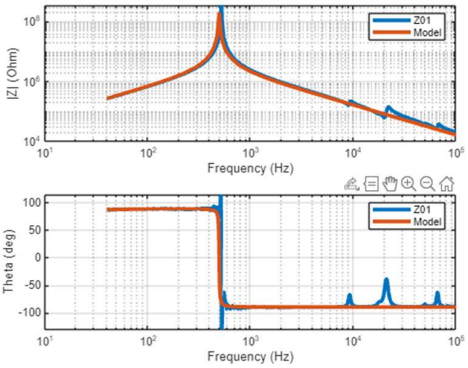

Fig.13.1. Simulation of Z01

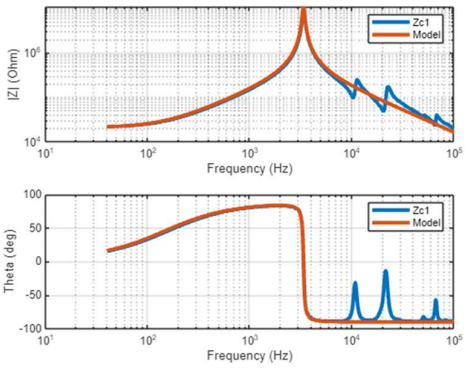

Fig.13.2. Simulation of ZC1

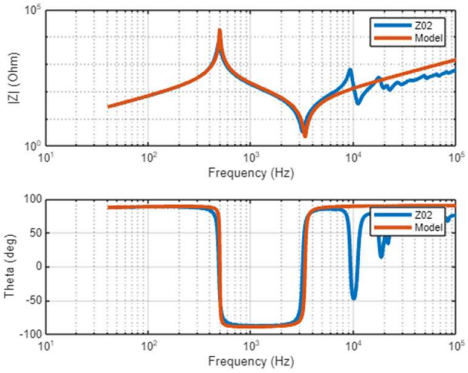

Fig.13.3. Simulation of Z02

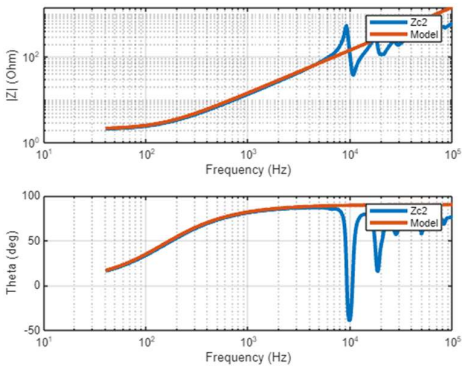

Fig.13.4. Simulation of ZC2

6. Modeling Discussion and Comparison

The tables 3 and 4 summarize the results of the procedure described in Section 5.2, applied to all prototypes listed in Table 1. The results show that the inductive system is highly dependent on the core characteristics. As observed, the nanocrystalline core exhibits high permeability, which shifts the resonance frequency to the left, as shown in Figures 6.1, 6.2, and 6.6. Regarding the inductive system, maintaining a similar winding geometry generally results in a comparable capacitive system. However, for Prototype E, there is a noticeable increase in capacitance accompanied by a decrease in inductance. Despite these changes, the overall behavior and resonance frequency of the system remain similar to those of the other prototypes. This is due to the relatively minor influence of such variations, the dominant parameter governing the circuit's impedance is the winding geometry.

Table 3. Inductive system parameters for all prototypes.

	$L_m[H]$	$L_{f\,BF}\ [mH]$	$L_{f\,HF}\ [mH]$
A	1048.98	2.15	0.95
B	1776.90	1.08	0.58
C	1180.80	3.02	1.96
D	42875.30	2.22	0.88
E	362.52	3.10	0.17

Table 4. Inductive system parameters for all prototypes.

	$C_1[pF]$	$C_2\ [pF]$	$C_3\ [pF]$
A	59.17	224.43	28.42
B	73.37	243.35	10.39
C	75.64	80.70	9.29
D	55.75	205.27	11.17
E	214.85	322.95	20.52

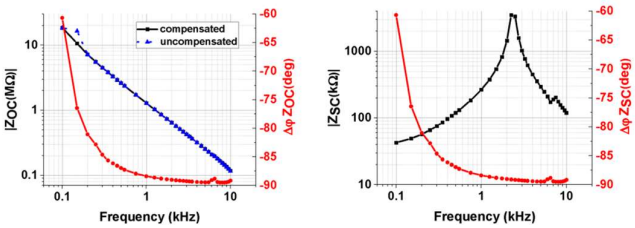

Fig.14. Results of impedence analysis through alternative measuring method in open and short circuit test. From [4]

As stated in [4] and confirmed by their experimental observations, the open-circuit test reveals a predominantly capacitive behavior in a portion of the transformer's impedance response, as shown in Figure 14. This effect arises from the high inductance and resulting high magnetizing voltage, which shift the impedance curve toward lower frequencies, making the capacitive component more prominent.

In the short-circuit test, the removal of the magnetic core's influence leads to a sharp drop in inductance. While [4] reported similar observations, it did not provide an interpretation of the frequency-dependent behavior, focusing only on direct voltage and current measurements rather than analyzing impedance over a frequency sweep. Despite the methodological differences, the strong resemblance in results supports the validity of our measurement approach.

7. Conclusion

In this work, a method originally developed for characterizing high-frequency (HF) transformers, typically operating with impedance resonances above 100 kHz was successfully adapted and applied to low-frequency IVTs, whose impedance resonance occurs below 1 kHz. The objective was to determine the elements of the equivalent electrical circuit and analyze the inductive and capacitive behavior of various IVT prototypes over a wide frequency range.

The method proved to be effective and was validated through circuit simulations, which confirmed its ability to accurately reproduce the frequency-dependent impedance behavior observed in measurements. While other studies have investigated the impedance response of IVTs and reported similar trends, they often stopped at observational conclusions without interpreting the underlying frequency phenomena. This highlights the added value of the proposed modeling approach.

The next phase of this research will focus on a more operationally relevant evaluation of IVTs by injecting a fundamental rated voltage signal superimposed with harmonic components, to further understand their behavior under real-world conditions.

8. References

[1] M. Kaczmarek et E. Stano, «Challenges of Accurate Measurement of Distorted Current and Voltage in the Power Grid by Conventional Instrument Transformers,» *Energies,* vol. 16, p. 2648, March 2023.

[2] J.-P. Keradec, «Transformateurs HF à enroulements-Schémas à constantes localisées,» 2008.

[3] J.-P. Kéradec, «Transformateurs HF à enroulements-Identification expérimentale,» 2009.

[4] D. Giordano, G. Crotti, P. S. Letizia et D. Palladini, «Stray Parameter Evaluation of Voltage Transformers for PQ Measurement in MV Applications,» chez *2022 20th International Conference on Harmonics & Quality of Power (ICHQP)*, 2022.

[5] A. Schellmanns, «Circuits équivalents pour transformateurs multienroulements : Application à la CEM conduite d'un convertisseur,» 1999.